Data-Driven Modeling in Geomechanics

Konstantinos Karapiperis

ETH Zürich

The theoretical framework of data-driven computational mechanics presents an alternative formulation of mechanics, whereby optimal material states are sought within a dataset that most closely satisfy momentum and energy conservation principles. We review the framework for the case of simple and nonsimple (polar), elastic and inelastic media, which represent common descriptions for geomaterials. Data mining from experiments and high-fidelity lower-scale simulations (DEM,FEM) are discussed, while remedies for data scarcity (adaptive data sampling) are also highlighted. Representative examples of a flat punch indentation and a rupture through a soil layer are presented, and a link to open-source Python code is provided.

1 Introduction

Predictive models in geomechanics have traditionally relied on continuum modeling via the formulation constitutive equations [DL82, MA91, VA91, OP04, DM04, DN05, BA06, HP06], discrete particle-based models [CS79, Bar94, KAVA18], as well as multiscale techniques that bridge the continuum and discrete scales [CMNN81, NDR05, KRB07, AT09, GZ14, RY11]. Initially informed by macroscopic experiments [RSW58, Ros70], and later by high-fidelity grain-scale resolved experiments [HBD$^+$10, AHV$^+$12], these models have been succesful in capturing essential aspects of granular materials and, more generally, geomaterials including pressure-dependent elasticity, history-dependence and critical state, fabric evolution, nonlocality. Despite their success, further progress has been hindered by numerous challenges including the uncertainty related to the models at different scales, as well as their complexity and the associated laborious process of calibration.

Recently, a variety of data-driven approaches have been developed in order to tackle the challenges outlined above, most importantly the bias, complexity or inefficiency of these methods, while incorporating information about the underlying mechanics and physics. These include physics-informed neural networks [HRM$^+$21] with a built-in structure of elastoplasticity [EPW22, HAV23, VS23], or with incorporated thermodynamics constraints [MSVMB21, HHR22]. Despite the physical basis of these models,

they are often hard to interpret, and could suffer from generalization errors for unseen stress-strain paths. An alternative approach which is not based on learning a constitutive law, but rather relies directly on the raw data is furnished by the framework of Data-Driven Computational Mechanics (DDCM), introduced Ortiz and co-workers. In DDCM, the mechanical problem is reformulated in terms of distances between a material dataset obtained from experiments, and an equilibrium set where the states that satisfy the physics reside. The method has been extended in various directions including inelasticity [EKR$^+$19], nonlocality [KOA21], stochasticity [PRO23], fracture [CDLSO20] and breakage mechanics [UGK$^+$23], and has been coupled with model-based approches [BS21] and machine-learning techniques [ESOR21, BS22] have also been developed in an effort to boost the efficiency and robustness of the method. The source of the data can be experiments [LCR$^+$18] or high-fidelity micromechanical calculations [KSOA20].

The chapter is organized as follows. In Section 2.1, the framework of data-driven mechanics is presented for simple continua, which is then extended to micropolar continua with a microstructure in Section 2.2. The enhancement of the framework to inelasticity is addressed in Section 2.3. Then, the source of data (experiments, micromechanical simulations) is discussed (Section 2.4), focusing also on data scarcity and how it can be efficiently overcome. We finish with representative examples and a link to an open-source code repository (Section 3).

2 Data-Driven Computational Mechanics

2.1 Cauchy Continuum - Elasticity

Let's first restrict our attention to the geometrically linear mechanical problem of a *simple* (nonlinear) elastic body that is discretized into N nodes and M material points (Fig 1). The body is subject to applied forces $\mathbf{f} = \{\mathbf{f}^\alpha\}_{\alpha=1}^N$, and undergoes displacements $\mathbf{u} = \{\mathbf{u}^\alpha\}_{\alpha=1}^N$ at its nodes. The state of each material point is described by a stress-strain pair indicating a point in the local phase space i.e., $\mathbf{z}^e = (\boldsymbol{\varepsilon}^e, \boldsymbol{\sigma}^e) \in Z^e$, and the state of the entire system is collectively a point in the global phase space $\mathbf{z} = \{\mathbf{z}^e\}_{e=1}^M \in Z$. The system is subject to the following discretized compatibility and equilibrium constraints:

$$\varepsilon_{ij}^e = \frac{1}{2}\sum_\alpha \left(N_{,j}^{e\alpha} u_i^\alpha + N_{,i}^{e\alpha} u_j^\alpha\right), \qquad e = 1, \dots, M \tag{1}$$

$$\sum_{e=1}^M w_e \sigma_{ij}^e N_{,j}^{e\alpha} = f_i^\alpha, \qquad \alpha = 1, \dots, N \tag{2}$$

where N^{ea} is the shape function of node α evaluated at the material point e within a finite element approximation scheme, and $\{w_e\}_{e=1}^M$ are elements of volume. The set of global states satisfying the above constraints define the equilibrium set E.

Instead of relying on a constitutive relation of the form $\boldsymbol{\sigma}^e = \boldsymbol{\sigma}^e(\boldsymbol{\varepsilon}^e)$ for closure, the Data-Driven formulation of the problem consists of finding the global state $\mathbf{z}$ that satisfies the compatibility and equilibrium constraints and, at the same time, minimizes the distance to a given material data set D. Therefore, the local phase spaces Z_e are equipped with an appropriate metric:

$$|\mathbf{z}^e| = \mathbb{C}^e\, \boldsymbol{\varepsilon}^e \cdot \boldsymbol{\varepsilon}^e + \mathbb{C}^{e^{-1}} \boldsymbol{\sigma}^e \cdot \boldsymbol{\sigma}^e \tag{3}$$

where $\mathbb{C}^e$ is a symmetric positive-definite tensor. Although the purpose of this tensor is numerical, and does not represent actual material behavior, it is typically given as the isotropic linear elasticity tensor:

$$\mathbb{C}^e_{ijkl} = \lambda \delta_{ij}\delta_{kl} + \mu(\delta_{ik}\delta_{jl} + \delta_{il}\delta_{jk}) \tag{4}$$

Note that this introduces two parameters λ, μ to the problem, the choice of which may generally affect how well the comparibility or equilibrium constraints are satisfied. To avoid this issue, and at the same time, obtain a parameter-free scheme, one can alternatively introduce a nested optimization problem within the definition of the distance as follows (e.g. [KOA21]):

$$|\mathbf{z}^e| = \min_{\lambda,\mu>0} \mathbb{C}^e(\lambda,\mu)\, \boldsymbol{\varepsilon}^e \cdot \boldsymbol{\varepsilon}^e + \mathbb{C}^{e^{-1}}(\lambda,\mu) \boldsymbol{\sigma}^e \cdot \boldsymbol{\sigma}^e \tag{5}$$

In the following, we will assume that a constant $\mathbb{C}^e$ is used, for the definition of the distance in the phase space. As a result, a metrization of the global phase space Z is induced by means of the norm:

$$|\mathbf{z}| = \sum_{e=1}^{N} w_e |\mathbf{z}^e|$$

The problem is mathematically formulated as:

$$\min_{\mathbf{y}\in D} \min_{\mathbf{z}\in E} |\mathbf{z} - \mathbf{y}| \tag{6}$$

where z denotes the *mechanical state* of the system i.e., the set of stress-strain pairs that satisfy equilibrium and compatibility, and y denotes the *material state* of the system i.e., the set of stress-strain pairs in the dataset.

The compatibility constraints are imposed by means of direct substitution, while the equilibrium constraints are enforced using Lagrange multipliers, resulting in the stationary problem:

$$\begin{aligned} \delta \Bigg[\sum_e w^e |z^e| \big(\frac{1}{2} \sum_\alpha \big(N^{e\alpha}_{,j} u^\alpha_i + N^{e\alpha}_{,i} u^\alpha_j\big), \sigma^e_{ij}\big) \\ - \sum_\alpha \big(\sum_e w_e \sigma^e_{ij} N^{e\alpha}_{,j} - f^\alpha_i \big) \eta^\alpha_i \Bigg] = 0 \end{aligned} \tag{7}$$

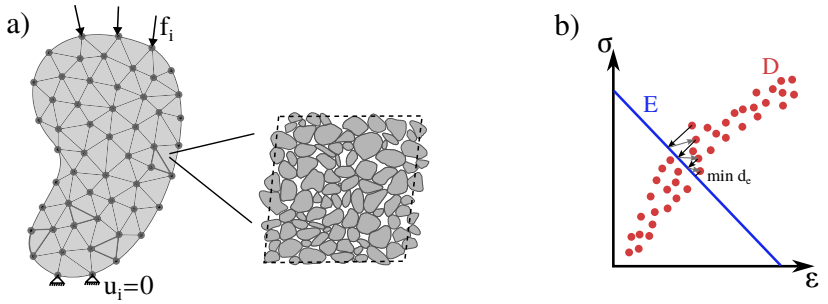

Figure 1: a) Simple continuum with granular microstructure. b) Illustration of the stress-strain states in the material data set (D), and their projections on the equilibrium set (E) with highlighted iterative procedure leading to a minimum distance solution.

Taking all possible variations $(\delta u_i^\alpha, \delta\sigma_{ij}^e, \delta\eta_i^a)$, and manipulating the resulting equations, one obtains a system of Euler-Lagrange equations [KO16]:

$$\sum_b \sum_e w_e C_{ijkl}^{e^*} N_{,j}^{e\alpha} N_{,l}^{eb} u_k^b = \sum_e w_e C_{ijkl}^{e^*} N_{,j}^{e\alpha} \varepsilon_{kl}^{e^*} \tag{8}$$

$$\sum_b \sum_e w_e C_{ijkl}^{e^*} N_{,j}^{e\alpha} N_{,l}^{eb} \eta_k^b = f_i^\alpha - \sum_e w_e N_{,j}^{e\alpha} \sigma_{ij}^{e^*} \tag{9}$$

where $\mathbf{z}^{e^*} = (\boldsymbol{\varepsilon}^{e^*}, \boldsymbol{\sigma}^{e^*})$ are the optimal local data points in the data set D^e that result in the closest possible satisfaction of the constraints. Eqs 8 and 9 represent two standard linear elasticity problems, one in terms of $\mathbf{u}$, and one in terms of $\boldsymbol{\eta}$.

Solution algorithm
Note that the optimal local points $\mathbf{y}^e = (\boldsymbol{\varepsilon}^{e^*}, \sigma^{e^*})$ in the data set D^e are not known a priori, which therefore calls for an iterative solution scheme. The simplest algorithm involves a fixed point iteration, where a fixed material state $\mathbf{y}^{(k)}$ is projected onto E (i.e. Eqs 8, 9 are solved) to obtain the updated mechanical state $\mathbf{z}^{(k)}$, where k denotes the iteration number. Then a search through the data set is carried out to find the closest material state $\mathbf{y}^{(k+1)}$, and the process is repeated until the material states remain unchanged. For more details the interested reader is referred to [KO16, KSOA20].

2.2 Micropolar continuum - Elasticity

The simple or Cauchy continuum is known to have limitations when it comes to modeling geomaterials especially in the failure regime (shear localization), due to the absence of an internal length scale [MV87]. In this section we describe the extension of the data-driven computational mechanics framework to the micropolar continuum, following [KOA21]. We therefore proceed to consider the mechanical problem of a (nonlinear) elastic micropolar body that is discretized into N nodes and M material points, similar to Section 2.1. However, the body is now subject to not only applied

forces $\mathbf{f} = \{\mathbf{f}^\alpha\}_{\alpha=1}^N$ but also moments $\mathbf{m} = \{\mathbf{m}^\alpha\}_{\alpha=1}^N$ (Fig. 2). Its kinematics are described by displacements $\mathbf{u} = \{\mathbf{u}^\alpha\}_{\alpha=1}^N$ and microrotations $\boldsymbol{\theta} = \{\theta^\alpha\}_{\alpha=1}^N$ at its nodes. Analogously, The state of each material point is described by a stress-strain pair $(\boldsymbol{\varepsilon}^e, \boldsymbol{\sigma}^e)$ and couple stress-curvature pair $(\boldsymbol{\kappa}^e, \boldsymbol{\mu}^e)$, which alltogether constitute a point in the local phase space i.e., $\mathbf{z}^e = (\boldsymbol{\varepsilon}^e, \boldsymbol{\kappa}^e, \boldsymbol{\sigma}^e, \boldsymbol{\mu}^e)$, and the state of the entire system is collectively a point in the global phase space $\mathbf{z} = \{\mathbf{z}^e\}_{e=1}^M \in Z$. The micropolar system is subject to the following discretized compatibility and equilibrium constraints:

$$\varepsilon_{ij}^e = \sum_\alpha \left(N_{,j}^{e\alpha} u_i^\alpha + \epsilon_{ijk} N^{e\alpha} \theta_k^\alpha\right), \qquad e = 1, \ldots, M \tag{10}$$

$$\kappa_{ij}^e = \sum_\alpha N_{,j}^{e\alpha} \theta_i^\alpha, \qquad e = 1, \ldots, M \tag{11}$$

$$\sum_{e=1}^M w_e \sigma_{ij}^e N_{,j}^{e\alpha} = f_i^\alpha, \qquad \alpha = 1, \ldots, N \tag{12}$$

$$\sum_{e=1}^M w_e \left(\mu_{ij}^e N_{,j}^{e\alpha} + \epsilon_{ijk} \sigma_{jk}^e N^{e\alpha}\right) = m_i^\alpha, \qquad \alpha = 1, \ldots, N \tag{13}$$

where, besides the quantities already introduced in Section **??**, ϵ_{ijk} is the third-order permutation tensor. The set of global states satisfying the above constraints define the equilibrium set E.

Analogously, we assume that a data set D is available, where material states reside. The micropolar formulation of the data-driven problem involes finding the global state $\mathbf{z}$ that satisfies the compatibility and equilibrium constraints and, at the same time, minimizes the distance to the material data set. To this end, we shall extend the metric introduced in the Cauchy continuum, to account for the additional kinematic and conjugate kinetic measures present in the micropolar continuum:

$$|\mathbf{z}^e| = \mathbb{C}^e\, \boldsymbol{\varepsilon}^e \cdot \boldsymbol{\varepsilon}^e + \mathbb{D}^e\, \boldsymbol{\kappa}^e \cdot \boldsymbol{\kappa}^e + \mathbb{C}^{e^{-1}} \boldsymbol{\sigma}^e \cdot \boldsymbol{\sigma}^e + \mathbb{D}^{e^{-1}}\, \boldsymbol{\mu}^e \cdot \boldsymbol{\mu}^e \tag{14}$$

where $\mathbb{C}^e$, $\mathbb{D}^e$ are the isotropic micropolar elasticity tensors, which once again do not reflect actual material properties, but are introduced for solely distance-inducing purposes:

$$\mathbb{C}_{ijkl}^e = \lambda \delta_{ij} \delta_{kl} + (\mu + \kappa) \delta_{ik} \delta_{jl} + (\mu - \kappa) \delta_{il} \delta_{jk} \tag{15}$$

$$\mathbb{D}_{ijkl}^e = \alpha \delta_{ij} \delta_{kl} + (\gamma + \beta) \delta_{ik} \delta_{jl} + (\gamma - \beta) \delta_{il} \delta_{jk} \tag{16}$$

The Data-Driven problem retains the the same mathematical formulation as in the Cauchy problem:

$$\min_{\mathbf{y} \in D} \min_{\mathbf{z} \in E} |\mathbf{z} - \mathbf{y}| \tag{17}$$

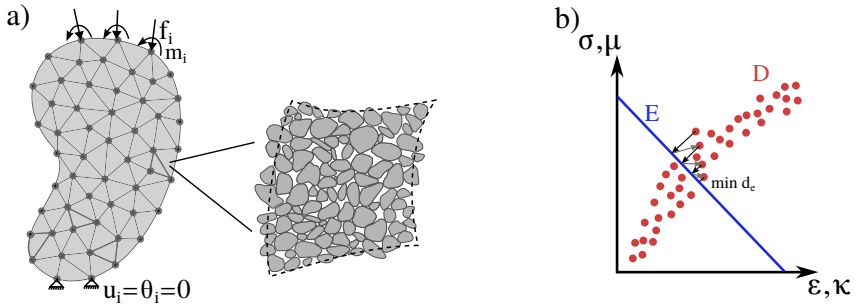

Figure 2: a) Micropolar continuum with granular microstructure. b) Illustration of the stress-strain states in the material data set (D), and their projections on the equilibrium set (E) with highlighted iterative procedure leading to a minimum distance solution.

with the difference that the state space has higher dimensions, due to the presence of the additional conjugate quantities related to the field of microrotations.

The stationary problem reads:

$$\delta\Bigg[\sum_e w^e|z^e|\Big(\sum_\alpha N^{e\alpha}_{,j}u^\alpha_i+\sum_\alpha \epsilon_{ijk}N^{e\alpha}\theta^\alpha_k,\sum_\alpha N^{e\alpha}_{,j}\theta^\alpha_i,\sigma^e_{ij},\mu^e_{ij}\Big) \tag{18}$$
$$-\sum_\alpha\Big(\sum_e w_e\sigma^e_{ij}N^{e\alpha}_{,j}-f^\alpha_i\Big)\eta^\alpha_i-\sum_\alpha\Big(\sum_e w_e(\mu^e_{ij}N^{e\alpha}_{,j}+\epsilon_{ijk}\sigma^e_{jk}N^{e\alpha})-m^\alpha_i\Big)\zeta^\alpha_i\Bigg]=0$$

Taking all possible variations ($\delta u^\alpha_i,\delta\theta^\alpha_i,\delta\sigma^e_{ij},\delta\mu^e_{ij},\delta\eta^a_i,\delta\zeta^a_i$), we obtain the following system of coupled Euler-Lagrange equations:

$$\sum_b\sum_e w_e\big(C^e_{ijkl}N^{e\alpha}_{,j}N^{eb}_{,l}u^b_k+C^e_{ijkl}N^{e\alpha}_{,j}N^{eb}\epsilon_{klm}\theta^b_m\big)=\sum_e w_eC^{e^*}_{ijkl}N^{e\alpha}_{,j}\varepsilon^{e^*}_{kl} \tag{19}$$
$$\sum_b\sum_e w_e\big[C^e_{ijkl}N^{e\alpha}N^{eb}_{,l}\epsilon_{ijm}u^b_k+\big(C^e_{ijkl}\epsilon_{ijm}\epsilon_{kln}N^{e\alpha}N^{eb}+D^{e^*}_{mjnl}N^{e\alpha}_{,j}N^{eb}_{,l}\big)\theta^b_n\big]$$
$$=\sum_e w_e\big(C^e_{ijkl}\epsilon_{ijm}N^{e\alpha}\epsilon^{e^*}_{kl}+D^e_{mjkl}N^{e\alpha}_{,j}\kappa^{e^*}_{kl}\big) \tag{20}$$
$$\sum_b\sum_e w_e\big(C^e_{ijkl}N^{eb}_{,j}N^{e\alpha}_{,l}\eta^b_i+C^e_{ijkl}N^{eb}N^{e\alpha}_{,l}\epsilon_{kij}\zeta^b_k\big)=f^\alpha_k-\sum_e w_eN^{e\alpha}_{,l}\sigma^{e^*}_{kl} \tag{21}$$
$$\sum_b\sum_e w_e\big[C^e_{ijkl}N^{e\alpha}N^{eb}_{,l}\epsilon_{ijm}\eta^b_k+\big(C^e_{ijkl}\epsilon_{ijm}\epsilon_{kln}N^{e\alpha}N^{eb}+D^e_{mjnl}N^{e\alpha}_{,j}N^{eb}_{,l}\big)\zeta^b_n\big]$$
$$=m^\alpha_m-\sum_e w_e\big(N^{e\alpha}_{,l}\mu^{e^*}_{ml}+\epsilon_{mkl}N^{e\alpha}\sigma^{e^*}_{kl}\big) \tag{22}$$

where $\mathbf{z}^{e^*}=(\boldsymbol{\varepsilon}^{e^*},\boldsymbol{\kappa}^{e^*},\boldsymbol{\sigma}^{e^*},\boldsymbol{\mu}^{e^*})$ are the optimal local data points in the data set D^e that result in the closest possible satisfaction of the constraints. Eqs (19,20) and

(21,22) represent two micropolar linear elasticity problems, one in terms of $\mathbf{u}, \boldsymbol{\theta}$, and one in terms of $\boldsymbol{\eta}, \boldsymbol{\zeta}$.

2.3 Extension to inelasticity

Practical applications in geomechanics often concern deformations beyond the elastic regime, which involve history-dependence and irreversibility. For conciseness we will present the extension to inelasticity for the Cauchy problem, but the inelastic extension for the micropolar problem follows analogously [KOA21]. To this end, we attend to a time-discrete formulation, whereby the Data-Driven problem of at time t_{k+1} reads:

$$\min_{\mathbf{y}_{k+1} \in D_{k+1}} \min_{\mathbf{z}_{k+1} \in E_{k+1}} |\mathbf{z}_{k+1} - \mathbf{y}_{k+1}| \tag{23}$$

where $\mathbf{z}_{k+1} = \{\mathbf{z}^e_{k+1}\}_{e=1}^M \in Z$ and $\mathbf{z}^e_{k+1} = (\boldsymbol{\varepsilon}^e_{k+1}, \boldsymbol{\sigma}^e_{k+1})$. The time-dependent constraint set E_{k+1} arises from the time-dependent applied forces $\mathbf{f}_{k+1}$. Accordingly, the behavior at a material point is described by a material data set D^e_{k+1} of points that is attainable at time t_{k+1} given its past local history of deformation:

$$D^e_{k+1} = \{(\boldsymbol{\varepsilon}^e_{k+1}, \boldsymbol{\sigma}^e_{k+1}) \,|\, \text{past history}\} \tag{24}$$

In practical terms, this implies that one has to deal with evolving material data sets. The conceptually simplest yet computationally expensive parametrization of the history relies on keeping a (potentially truncated) memory of the strain history at a material point [EKR$^+$19]. This mathematically translates to:

$$D^e_{k+1} = \{(\boldsymbol{\varepsilon}^e_{k+1}, \boldsymbol{\sigma}^e_{k+1}) \,|\, \{\boldsymbol{\varepsilon}^e_l\}_{l \leq k}\} \tag{25}$$

which resembles a data-driven formulation focusing on trajectories – rather than points – in stress-strain space.

An alternative approach relies on enhancing the state space with a suitable set of internal variables $\boldsymbol{q}$, which represent the evolving internal structure of the material at hand, and encapsulates its history [KSOA20, EKR$^+$19]. In this case, the material data set admits the parametrization:

$$D^e_{k+1} = \{(\boldsymbol{\varepsilon}^e_{k+1}, \boldsymbol{\sigma}^e_{k+1}) \,|\, (\boldsymbol{\varepsilon}^e_k, \boldsymbol{\sigma}^e_k, \boldsymbol{q}^e_k)\} \tag{26}$$

The internal variable parametrization outlined above can be replaced or enhanced with an energy-based parametrization, whereby the state space is augmented with the free energy $\mathcal{A}$ and dissipation $\mathcal{D}$, which are related to the state variables $\boldsymbol{\epsilon}, \boldsymbol{\sigma}$ via the principle of conservation of energy and the second principle (Clausius-Plank inequality), stated in a time-discrete setting as:

$$\mathcal{D}^e_{k+1} - \mathcal{D}^e_k = \frac{\boldsymbol{\sigma}^e_k + \boldsymbol{\sigma}^e_{k+1}}{2} : (\boldsymbol{\epsilon}^e_{k+1} - \boldsymbol{\epsilon}^e_k) - (\mathcal{A}^e_{k+1} - \mathcal{A}^e_k) \geq 0 \tag{27}$$

The local material data set at time t_{k+1} is then represented as:

$$D^e_{k+1} = \{(\boldsymbol{\epsilon}^e_{k+1}, \boldsymbol{\sigma}^e_{k+1}) \,|\, (\boldsymbol{\epsilon}^e_k, \boldsymbol{\sigma}^e_k), (27)\} \tag{28}$$

The above relation states that the admissible stress-strain pairs at time t_{k+1} are those that are thermodynamically consistent with the material state at time t_k. The special case where $\mathcal{D}^e_{k+1} - \mathcal{D}^e_k = 0$ defines a bounded equilibrium set (or elastic domain) on the augmented state space. More details about the various options for history parametrization can be found in [EKR$^+$19, KSOA20]. Note that in the case of the internal variable and energy-based parametrization, the necessary quantities can be obtained directly from lower scale models, e.g., as we will address in Section 2.4.

Regardless of the particular choice of parametrization of the local material data sets, the global material data set then follows as:

$$D_{k+1} = D^1_{k+1} \times \ldots \times D^M_{k+1} \tag{29}$$

2.4 Data sampling

So far, we have assumed that material data are available, but we have not addressed the source of the data, or their potential scarcity. In principle, data can be obtained from various sources, either experimental or computational, and potentially combined within the same simulation. The experimental identification of material data sets has been addressed in [LCR$^+$18], whereby a database of stress-strain couples is compiled from a given displacement field – obtained though imaging techniques – and known boundary conditions, by solving a distance minimization problem (Fig. 3 a). Alternatively, data can be compiled from high-fidelity lower scale simulations [KSOA20], which for geomechanical problems typically amount to discrete element models in case of granular assemblies, or finite element models of heterogeneous porous materials (Fig. 3 b). This approach gives rise a multiscale interpretation of data-driven computing. In the latter case, homogenization principles shall be used to derive the macroscopic quantities that describe the material states (stress, structural variables, energetical quantities). These principles are reviewed below in the case of discrete assemblies (e.g. granular media) and continuum representative volume elements (e.g. porous rocks).

Homogenization of granular ensemblies
In the case where *discrete* element simulations (e.g. [KHA$^+$20]) are used for the purpose of generating the data, then the macroscopic material states (stress, strain, free energy, dissipation, microstructural variables) need to be obtained from the discrete quantities (particle displacements, interparticle forces). Assuming quasi-static conditions, the average stress tensor of the granular assembly is given by [CMNN81]:

$$\boldsymbol{\sigma} = \frac{1}{V} \sum_c \mathbf{f}^c \otimes \mathbf{l}^c \tag{30}$$

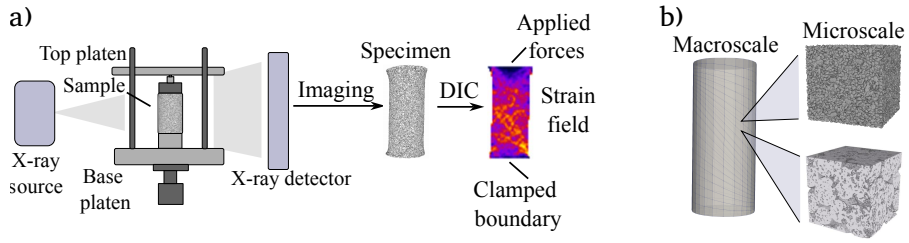

Figure 3: a) Identification of material data sets from in-situ experiment. b) Material data sets extracted from micromechanical RVEs, with examples showing a granular ensemble and a porous rock.

where the summation is performed over all contacts c of all particles in the assembly (unit cell), $\mathbf{f}^c$ is the interparticle force, and $\mathbf{l}^c$ is the branch vector connecting the centroids of contacting particles, and V is the volume of the granular assembly. The average strain $\boldsymbol{\varepsilon}$ is obtained from the boundary deformation of the unit cell, and the free energy density due to local deformation at the contacts is given by:

$$\mathcal{A} = \sum_c \mathcal{A}^c = \frac{1}{2V} \sum_c \left(\frac{\|\mathbf{f}_n^c\|^2}{k_n} + \frac{\|\mathbf{f}_t^c\|^2}{k_t} \right) \tag{31}$$

where k_n, k_t are the normal and tangential contact stiffnesses at an interparticle frictional contact, respectively, and $\mathbf{f}_n^c, \mathbf{f}_t^c$ are the normal and tangential components of the interparticle force.

The dissipation can be computed incrementally by energy balance:

$$d\mathcal{D} = \boldsymbol{\sigma} : d\boldsymbol{\varepsilon} - d\mathcal{A} \tag{32}$$

or, from the frictional slip at the interparticle contacts,

$$d\mathcal{D} = \sum_c d\mathcal{D}^c = \frac{1}{V} \sum_c \mathbf{f}_t^c \cdot d\mathbf{u}^{c,\,\mathrm{slip}} \tag{33}$$

where $d\mathbf{u}^{c,\,\mathrm{slip}} = (\mathbf{f}_t^{c,t} - \mathbf{f}_t^{c,t+dt})/k_t$.

Microstructural measures acting as internal variables augmenting the state space (Section 2.3) may similarly be obtained by averaging microscopic quantities. For example, the commonly used contact normal fabric tensor [Oda72]:

$$\boldsymbol{F} = \frac{1}{2N_c} \sum_c \boldsymbol{n}^c \otimes \boldsymbol{n}^c \tag{34}$$

where N_c is the number of contacts in the assembly, and $\boldsymbol{n}^c$ is the contact normal vector. Analogous quantities can be obtained for nonsimple (polar) continua, as discussed in [KOA21].

Homogenization of heterogeneous porous geomaterials

In the case where *continuum* microstructural RVEs are used to generate material data sets, then similar principles apply. Assuming quasistatic conditions, the average stress tensor of the micromechanical RVE is given as:

$$\boldsymbol{\sigma} = \frac{1}{V} \int_{\partial V} \mathbf{t} \otimes \mathbf{x} \, dS \tag{35}$$

where $\mathbf{t}$ denotes the traction acting on the boundary of the continuum RVE, and $\mathbf{x}$ denotes the position of the material point on the boundary.

The free energy, and dissipation are given simply by averaging, and energy balance respectively:

$$\mathcal{A} = \int_V \mathcal{A}(\mathbf{x}) \, d\mathbf{x} \tag{36}$$

$$d\mathcal{D} = \boldsymbol{\sigma} : d\boldsymbol{\varepsilon} - d\mathcal{A} \tag{37}$$

while continuum texture tensors, similar to Eq. 34, may analogously be defined.

Adaptive sampling

In the above, it was assumed that micromechanical calculations are carried out along predetermined stress paths. In practice, these predetermined paths may not sufficiently cover the state space as needed for a specific application or boundary value problem.

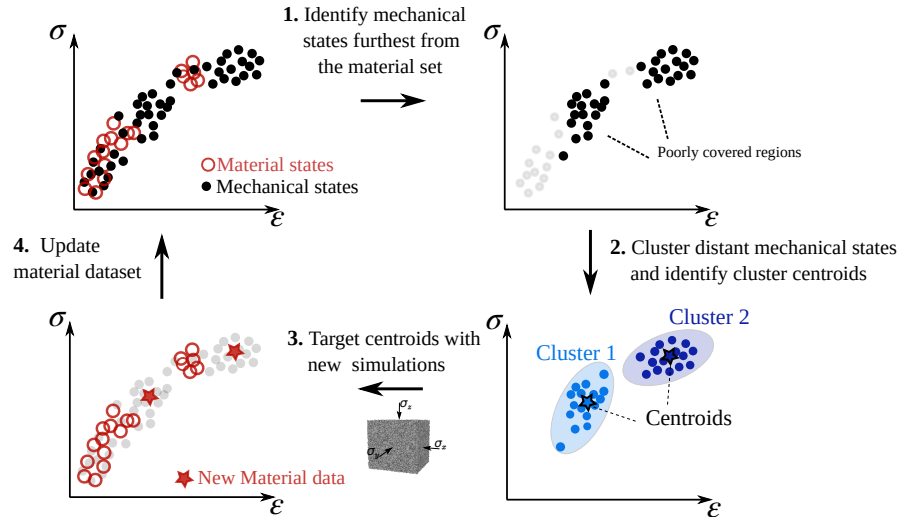

Figure 4: Adaptive sampling procedure for multiscale data-driven computational mechanics.

In this case, we can leverage the formulation of data-driven computational mechanics as a distance minimization problem, and identify, using unsupervised learning, regions in state space with such poor data coverage. As shown in Fig. 4, these regions may then be targeted with additional experiments or lower-scale simulations, in an active learning manner. The result is a better coverage of the phase space for a given application or problem. The interested reader is referred to [GKS+23] for details on this adaptive sampling technique.

3 Applications

We present here two representative examples that leverage the theoretical and algorithmic depevelopments discussed above. The first one is a 2D flat punch indentation of a model elastic medium, as shown in Fig. 5 a). For simplicity, we restrict our attention to a simple and history-independent material behavior, by generating a dataset of $N = 10^6$ stress-strain pairs via evaluating an isotropic linear elastic law. The prediction was repeated using a sequence of successively larger datasets, until convergence of the predicted response was obtained. This convergence can be verified in Fig. 5 b), where the indenter force-displacement relation is plotted for increasing dataset size. The code needed to reproduce the example is openly available in the author's Github repository (github.com/kkarapiperis/ddcm-2D/). In the second example, shown in Fig. 5 c), a rupture propagates into a model granular material. In this case, the material behavior is furnished by the homogenized response of a discrete element assembly (Section 2.4), following the multiscale interpretation of the framework. The resulting surface deformation profile at the end of the simulation is shown in Fig. 5

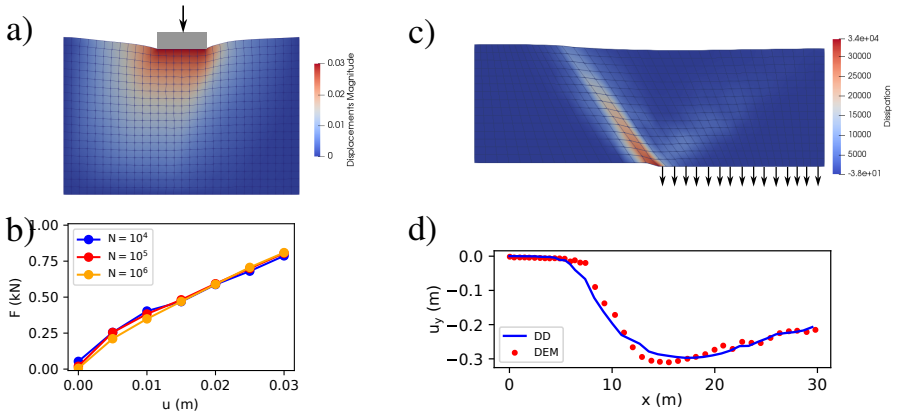

Figure 5: a) Example of a 2D flat punch indentation into an elastic medium. b) Indenter force-displacement curve prediction for increasing size of the dataset. c) Example of a fault rupture through a layer of model granular material. d) Predicted surface displacement profile, and comparison with a fully resolved discrete element simulation.

d), which compares well with a fully resolved discrete element simulation of the same problem.

4 Conclusions

In summary, the framework of data-driven computational mechanics, offers a novel avenue to solving problems in geomechanics, including challenging ones that involve failure and localized deformation. Free from the uncertainty of the classical constitutive modeling approach and the caveats of machine learning models, the data-driven formulation offers an alternative paradigm for computation. The need for large amounts of data represents a potential pitfall of the method, which may be addressed by the use of high-fidelity micromechanical simulations, augmenting data sets available from experiments. Finally, an additional remedy to the problem is furnished by the use of adaptive sampling techniques.

References

[AHV+12] E. Andò, S.A. Hall, G. Viggiani, J. Desrues, and P. Bésuelle. Grain-scale experimental investigation of localised deformation in sand: a discrete particle tracking approach. *Acta Geotechnica*, 7(1):1–13, Mar 2012.

[AT09] J. E. Andrade and X. Tu. Multiscale framework for behavior prediction in granular media. *Mechanics of Materials*, 41(6):652–669, 2009. Advances in the Dynamics of Granular Materials.

[BA06] R. I. Borja and J. E. Andrade. Critical state plasticity. part vi: Meso-scale finite element simulation of strain localization in discrete granular materials. *Computer Methods in Applied Mechanics and Engineering*, 195(37–40):5115–5140, 2006. John H. Argyris Memorial Issue. Part I.

[Bar94] J.P. Bardet. Numerical simulations of the incremental responses of idealized granular materials. *International Journal of Plasticity*, 10(8):879–908, 1994.

[BS21] Bahador Bahmani and WaiChing Sun. A kd-tree-accelerated hybrid data-driven/model-based approach for poroelasticity problems with multi-fidelity multi-physics data. *Computer Methods in Applied Mechanics and Engineering*, 382:113868, 2021.

[BS22] Bahador Bahmani and WaiChing Sun. Manifold embedding data-driven mechanics. *Journal of the Mechanics and Physics of Solids*, 166:104927, 2022.

[CDLSO20] Pietro Carrara, Laura De Lorenzis, Laurent Stainier, and Michael Ortiz. Data-driven fracture mechanics. *Computer Methods in Applied Mechanics and Engineering*, 372:113390, 2020.

[CMNN81] J. Christoffersen, M. M. Mehrabadi, and S. Nemat-Nasser. A micromechanical description of granular material behavior. *Journal of Applied Mechanics*, 48(2):339–344, 1981.

[CS79] P. A. Cundall and O. D. L. Strack. A discrete numerical model for granular assemblies. *Géotechnique*, 29(1):47–65, 1979.

[DL82] F. Darve and S. Labanieh. Incremental constitutive law for sands and clays: Simulations of monotonic and cyclic tests. *International Journal for Numerical and Analytical Methods in Geomechanics*, 6(2):243–275, 1982.

[DM04] Y. F. Dafalias and M. T. Manzari. Simple plasticity sand model accounting for fabric change effects. *Journal of Engineering Mechanics*, 130(6):622–634, 2004.

[DN05] F. Darve and F. Nicot. On incremental non-linearity in granular media: Phenomenological and multi-scale views (part i). *International Journal for Numerical and Analytical Methods in Geomechanics*, 29(14):1387–1409, 2005.

[EKR+19] R. Eggersmann, T. Kirchdoerfer, S. Reese, L. Stainier, and M. Ortiz. Model-free data-driven inelasticity. *Computer Methods in Applied Mechanics and Engineering*, 350:81–99, 2019.

[EPW22] Mahdad Eghbalian, Mehdi Pouragha, and Richard Wan. A physics-informed deep neural network for surrogate modeling in classical elasto-plasticity. *arXiv preprint arXiv:2204.12088*, 2022.

[ESOR21] Robert Eggersmann, Laurent Stainier, Michael Ortiz, and Stefanie Reese. Model-free data-driven computamechanics enhanced by tensor voting. *Computer Methods in Applied Mechanics and Engineering*, 373:113499, 2021.

[GKS+23] Anna Gorgogianni, Konstantinos Karapiperis, Laurent Stainier, Michael Ortiz, and José E Andrade. Adaptive goal-oriented data sampling in data-driven computational mechanics. *Computer Methods in Applied Mechanics and Engineering*, 409:115949, 2023.

[GZ14] N. Guo and J. Zhao. A coupled fem/dem approach for hierarchical multiscale modelling of granular media. *International Journal for Numerical Methods in Engineering*, 99(11):789–818, 2014.

[HAV23] Ehsan Haghighat, Sahar Abouali, and Reza Vaziri. Constitutive model characterization and discovery using physics-informed deep learning. *Engineering Applications of Artificial Intelligence*, 120:105828, 2023.

[HBD+10] S.A. Hall, M. Bornert, J. Desrues, Y. Pannier, N. Lenoir, G. Viggiani, and P. Bésuelle. Discrete and continuum analysis of localised deformation in sand using x-ray ct and volumetric digital image correlation. *Géotechnique*, 60(5):315–322, 2010.

[HHR22] Shenglin Huang, Zequn He, and Celia Reina. Variational onsager neural networks (vonns): A thermodynamics-based variational learning strategy for non-equilibrium pdes. *Journal of the Mechanics and Physics of Solids*, 163:104856, 2022.

[HP06] G. T. Houlsby and A. M Puzrin. *Principles of Hyperplasticity*. Springer, 2006.

[HRM+21] Ehsan Haghighat, Maziar Raissi, Adrian Moure, Hector Gomez, and Ruben Juanes. A physics-informed deep learning framework for inversion and surrogate modeling in solid mechanics. *Computer Methods in Applied Mechanics and Engineering*, 379:113741, 2021.

[KAVA18] R. Kawamoto, E. Andò, G. Viggiani, and J. E. Andrade. All you need is shape: Predicting shear banding in sand with LS-DEM. *Journal of the Mechanics and Physics of Solids*, 111:375–392, 2018.

[KHA+20] Konstantinos Karapiperis, John Harmon, Edward Andò, Gioacchino Viggiani, and José E. Andrade. Investigating the incremental behavior of granular materials with the level-set discrete element method. *Journal of the Mechanics and Physics of Solids*, 144:104103, 2020.

[KO16] T. Kirchdoerfer and M. Ortiz. Data-driven computational mechanics. *Computer Methods in Applied Mechanics and Engineering*, 304:81–101, 2016.

[KOA21] K. Karapiperis, M. Ortiz, and J.E. Andrade. Data-driven nonlocal mechanics: Discovering the internal length scales of materials. *Computer Methods in Applied Mechanics and Engineering*, 386:114039, 2021.

[KRB07] K. Kamrin, C.H. Rycroft, and M. Z. Bazant. The stochastic flow rule: A multi-scale model for granular plasticity. *Modelling and Simulation in Materials Science and Engineering*, 15(4):S449, 2007.

[KSOA20] K. Karapiperis, L. Stainier, M. Ortiz, and J.E. Andrade. Data-driven multiscale modeling in mechanics. *Journal of the Mechanics and Physics of Solids*, page 104239, 2020.

[LCR+18] Adrien Leygue, Michel Coret, Julien Rethore, Laurent Stainier, and Erwan Verron. Data-based derivation of material response. *Computer Methods in Applied Mechanics and Engineering*, 331:184–196, 2018.

[MA91] H.-B. Mühlhaus and E.C. Alfantis. A variational principle for gradient plasticity. *International Journal of Solids and Structures*, 28(7):845–857, 1991.

[MSVMB21] Filippo Masi, Ioannis Stefanou, Paolo Vannucci, and Victor Maffi-Berthier. Thermodynamics-based artificial neural networks for constitutive modeling. *Journal of the Mechanics and Physics of Solids*, 147:104277, 2021.

[MV87] H. B. Mühlhaus and I. Vardoulakis. The thickness of shear bands in granular materials. *Géotechnique*, 37(3):271–283, 1987.

[NDR05] F. Nicot, F. Darve, and RNVO Group: Natural Hazards and Vulnerability of Structures. A multi-scale approach to granular materials. *Mechanics of Materials*, 37(9):980–1006, 2005.

[Oda72] M. Oda. Initial fabrics and their relation to mechanical properties of granular materials. *Soils and Foundations*, 12(1):17–36, 1972.

[OP04] M Ortiz and A Pandolfi. A variational cam-clay theory of plasticity. *Computer Methods in Applied Mechanics and Engineering*, 193(27):2645–2666, 2004. Computational Failure Mechanics for Geomaterials.

[PRO23] Erik Prume, Stefanie Reese, and Michael Ortiz. Model-free data-driven inference in computational mechanics. *Computer Methods in Applied Mechanics and Engineering*, 403:115704, 2023.

[Ros70] K. H. Roscoe. The influence of strains in soil mechanics. *Géotechnique*, 20(2):129–170, 1970.

[RSW58] K. H. Roscoe, A. N. Schofield, and C. P. Wroth. On the yielding of soils. *Géotechnique*, 8(1):22–53, 1958.

[RY11] Richard A. Regueiro and Beichuan Yan. Concurrent multiscale computational modeling for dense dry granular materials interfacing deformable solid bodies. In Richard Wan, Mustafa Alsaleh, and Joe Labuz, editors, *Bifurcations, Instabilities and Degradations in Geomaterials*, pages 251–273. Springer Berlin Heidelberg, Berlin, Heidelberg, 2011.

[UGK+23] Jacinto Ulloa, Anna Gorgogianni, Konstantinos Karapiperis, Michael Ortiz, and José E Andrade. Data-driven breakage mechanics: Predicting the evolution of particle-size distribution in granular media. *Journal of the Mechanics and Physics of Solids*, page 105328, 2023.

[VA91] I. Vardoulakis and E.C. Aifantis. A gradient flow theory of plasticity for granular materials. *Acta Mechanica*, 87(3):197–217, 1991.

[VS23] Nikolaos N Vlassis and WaiChing Sun. Geometric learning for computational mechanics part ii: Graph embedding for interpretable multiscale plasticity. *Computer Methods in Applied Mechanics and Engineering*, 404:115768, 2023.